Inorganic Chemistry
Article
Cite This: Inorg. Chem. 2018, 57, 13279−13288
pubs.acs.org/IC

Structure, Thermal Stability, and Spectroscopic Properties of Triclinic Double Sulfate $AgEu(SO_4)_2$ with Isolated SO_4 Groups

Yuriy G. Denisenko,[†,‡] Victor V. Atuchin,[*,§,∥] Maxim S. Molokeev,[⊥,#,¶] Aleksandr S. Aleksandrovsky,[□,○] Alexander S. Krylov,[△] Aleksandr S. Oreshonkov,[#,△] Svetlana S. Volkova,[†] and Oleg V. Andreev[†]

[†]Institute of Chemistry, Tyumen State University, Tyumen 625003, Russia
[‡]Department of General and Special Chemistry, Industrial University of Tyumen, Tyumen 625000, Russia
[§]Laboratory of Optical Materials and Structures, Institute of Semiconductor Physics, SB RAS, Novosibirsk 630090, Russia
[∥]Laboratory of Semiconductor and Dielectric Materials, Novosibirsk State University, Novosibirsk 630090, Russia
[⊥]Laboratory of Crystal Physics, Kirensky Institute of Physics, Federal Research Center KSC SB RAS, Krasnoyarsk 660036, Russia
[#]Siberian Federal University, Krasnoyarsk 660041, Russia
[¶]Department of Physics, Far Eastern State Transport University, Khabarovsk 680021, Russia
[□]Laboratory of Coherent Optics, Kirensky Institute of Physics, Federal Research Center KSC SB RAS, Krasnoyarsk 660036, Russia
[○]Institute of Nanotechnology, Spectroscopy and Quantum Chemistry, Siberian Federal University, Krasnoyarsk 660041, Russia
[△]Laboratory of Molecular Spectroscopy, Kirensky Institute of Physics, Federal Research Center KSC SB RAS, Krasnoyarsk 660036, Russia

Supporting Information

ABSTRACT: Silver−europium double sulfate $AgEu(SO_4)_2$ was obtained by solid-phase reaction between Ag_2SO_4 and $Eu_2(SO_4)_3$. The crystal structure of $AgEu(SO_4)_2$ was determined by Monte Carlo method with simulated annealing, and after that, it was refined by the Rietveld method from X-ray powder diffraction data. The compound crystallizes in the triclinic symmetry, space group $P\bar{1}$ (a = 0.632929(4), b = 0.690705(4), c = 0.705467(4) nm, α = 98.9614(4), β = 84.5501(4), γ = 88.8201(4)°, V = 0.303069(3) nm^3). Two types of sulfate tetrahedra were found in the structure, which significantly affects the spectroscopic properties in the IR-range. In the temperature range of 143−703 K, the average linear thermal expansion coefficients of cell parameters a, b, and c are very similar, $(1.11−1.67) \times 10^{-5}$ K^{-1} in magnitude, and therefore, $AgEu(SO_4)_2$ expands almost isotropically. Upon heating in argon flow, $AgEu(SO_4)_2$ is stable up to 1053 K. The luminescence spectra in the region of ultranarrow $^5D_0−^7F_0$ transition contain a single narrow and symmetric line at 579.5 nm that is evidence of good crystalline quality of $AgEu(SO_4)_2$ and uniform local environment of Eu^{3+} ions in the structure. Distribution of luminescence bands is determined by the environment of Eu^{3+} ions in the structure. Influence of Ag^+ ions on the electron density distribution at Eu sites is detected.

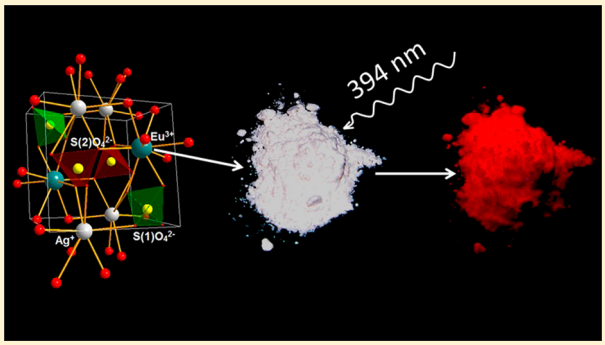

1. INTRODUCTION

In modern technologies, the oxide compounds of rare-earth elements (REE) are the basis for creating highly efficient polyfunctional materials with precise control of composition and micromorphology and reproducible characteristics.[1−6] A wide range of applications of rare earth compounds is generated by such factors as their specific electronic structure and spectroscopic properties and diverse crystal chemistry.[7−16] Among different chemical classes of REE crystals, the double salts formed by tetrahedral anions are of special scientific and technological interests. Indeed, many valuable laser and luminescence materials are created based on complex REE molybdate and tungstate hosts having tetrahedral groups MO_4 (M = Mo, W).[17−23] In the technology of separation, enrichment, and utilization of raw rare-earth materials, the double salts of rare-earth elements are extremely important.[24−31] Also, the double sulfates of rare-earth elements are of interest to researchers due to the catalytic property manifestation in oxidation−reduction processes.[32,33]

The compounds $A^ILn(SO_4)_2$ (A = Li, Na, K, Cs, NH_4) have been studied in the past, and crystal structures were defined for

Received: July 2, 2018
Published: October 15, 2018

DOI: 10.1021/acs.inorgchem.8b01837
Inorg. Chem. 2018, 57, 13279−13288

several sulfates.[8,34−44] The available structural information is shortly summarized in Table S1. It is evident that, depending on the selection of A and Ln cations, the different structures were observed in the $A^{I}Ln(SO_4)_2$ crystals. As based on the effective ion radii similarity, besides alkaline metals and ammonium, the formation of $Ag^{I}Ln(SO_4)_2$ compounds could be reasonably assumed. Indeed, the fragmentary report on the unit cell parameters of $AgPr(SO_4)_2$ and $AgEr(SO_4)_2$ sulfates was found in the literature.[8] The crystal structures or other properties of the compounds, however, cannot be found in the conventional sources. Hence, it could be concluded that the formation of $AgLn(SO_4)_2$ compounds is feasible, but information about possible synthesis routes, stability, and chemical and physical properties of these crystals is absent in the literature. Thus, the present study is aimed at the synthesis of $AgEu(SO_4)_2$ and evaluation of their structural, thermophysical, and spectroscopic properties. The selection of europium(III) for this experiment as a representative member of the Ln family is governed by several reasons. In the present photonics, the Eu^{3+}-bearing compounds are actively studied as red-light-emitting phosphors for the creation of efficient WLED sources.[5,9,45−49] Respectively, the spectroscopic characteristics of $AgEu(SO_4)_2$ are very interesting because, in this structure, the Eu^{3+} ions could be assumed to be in the specific low-symmetry coordination similarly to Ln^{3+} coordination in other related $A^{I}Ln(SO_4)_2$ (A = Na, K) crystals.[37−41] As it is known, the electronic transitions in Eu^{3+} ions are highly sensitive to the crystallographic environment.[50−53] Besides, the different sulfates of europium(III), due to the presence of two redox centers Eu^{3+} and SO_4^{2-}, can exhibit a catalytic effect on the oxidation and reduction reactions of organic compounds.[33,52,54]

2. EXPERIMENTAL METHODS

The double sulfate $AgEu(SO_4)_2$ was synthesized according to the solid-phase reaction:

$$Ag_2SO_4 + Eu_2(SO_4)_3 \rightarrow 2AgEu(SO_4)_2$$

Initially, $Eu_2(SO_4)_3$ was fabricated according to reactions:

$$Eu_2O_3 + 6HNO_3 \rightarrow 2Eu(NO_3)_3 + 3H_2O$$

$$2Eu(NO_3)_3 + 3H_2SO_4 \rightarrow Eu_2(SO_4)_3 \downarrow + 6HNO_3$$

After the precipitation reaction, the reaction mixture was evaporated to a dry residue. The resulting polycrystalline product was calcined at 723 K for 168 h in a muffle furnace. The obtained powder, according to X-ray diffraction and X-ray fluorescent analysis, was of pure europium sulfate III. According to the gravimetric analysis, the content of sulfate ions in the synthesized product was 48.66%, and the theoretical value is 48.65% for $Eu_2(SO_4)_3$. The possible error in the content determination is 0.02%, which does not exceed the value of the relative error for this method of analysis (0.15%).

High purity starting reagents were used for the synthesis: Ag_2SO_4 (ultrapure, Vekton Ltd., Russia) and Eu_2O_3 (99.99%, ultrapure, TDM-96 Ltd. Russia). The dry reagents weighing was carried out on an analytical balance with an accuracy of 0.1 mg. The stoichiometric sulfate charge was carefully ground in an agate mortar, and then, the mixture was transferred to an alumina crucible and treated in a muffle furnace at 923 K. The heat treatment was carried out for 12 h in the air atmosphere. The resulting cake was carefully ground in an agate mortar, and then, the heating procedure was repeated. After the annealing, the sample was cooled to room temperature together with the furnace. As seen in Figure S1, under illumination by sunlight, the synthesized $AgEu(SO_4)_2$ product possesses a light cream color, which is a general characteristic of Eu^{3+}-containing oxide compounds.[50,53]

The powder diffraction data for $AgEu(SO_4)_2$ structural analysis were collected at room temperature with a Bruker D8 ADVANCE powder diffractometer (Cu Kα radiation) and linear VANTEC detector. The 2θ range of 10−144° was measured with 0.6 mm divergence slit, the step size of 2θ was 0.016°, and the counting time was 5 s per step. Additional 15 XRD patterns were measured in the temperature range of 143−703 K using the Anton Paar/Bruker-AXS TTK-450 heat attachment. The 2θ range of 8−90° was measured with 1 mm divergence slit, the step size of 2θ was 0.016°, and the counting time was 0.3 s per step.

To see the particle morphology, scanning electron microscopy (SEM) was implemented with the use of electron microscope JEOL JSM-6510LV.

Thermal analysis was carried out in synthetic air (80% Ar, 20% O_2) flow using simultaneous thermal analysis (STA) equipment 499 F5 Jupiter NETZSCH (Germany). The powder samples were inserted into alumina crucibles. The heating rate was 5 K/min. The equipment was initially calibrated with the use of standard metal substances such as In, Sn, Zn, Al, Ag, Au, and Ni. The possible error in determining the temperature does not exceed 0.5%.

Fourier transform infrared spectroscopy (FTIR) was carried out using Fourier transform infrared spectrometer FSM 1201. The sample for the investigation was prepared in the form of a tablet with addition of annealed KBr at the weight ratio KBr:$AgEu(SO_4)_2$ = 100:1. The unpolarized Raman spectra were collected in backscattering geometry, using a triple Raman spectrometer Horiba Jobin Yvon T64000 operating in subtractive mode. The spectral resolution for the recorded Stokes side Raman spectra was set to ∼2 cm^{-1} (this resolution was achieved by using gratings with 1800 grooves/mm and 100 mm slits). The microscope system based on an Olympus BX41 microscope with an Olympus 50× objective lens f = 0.8 mm with numerical aperture (NA) = 0.75, which provides a focal spot diameter of about 2 μm on the sample.[55,56] Single-mode 514 nm Spectra-Physics Stabilite 2017 Ar^+ laser was used as an excitation light source. The laser power was adjusted to be 1 mW at the samples in order to avoid samples heating. The luminescence spectra under room temperature were registered on Horiba Jobin-Yvon T64000 spectrometer with the spectral resolution 2.7 cm^{-1}. The excitation wavelength was 514.5 nm that, despite the absence of exact resonance, was shown to be useful for measurements of high quality and high-resolution luminescence spectra of europium in oxide matrixes.[50] The Raman spectrum was fitted by Lorentzian line-shapes, and infrared spectrum was fitted by Gaussian profile functions.

3. RESULTS AND DISCUSSION

The X-ray diffraction pattern recorded for $AgEu(SO_4)_2$ is shown in Figure 1. All reflections of $AgEu(SO_4)_2$ compound were

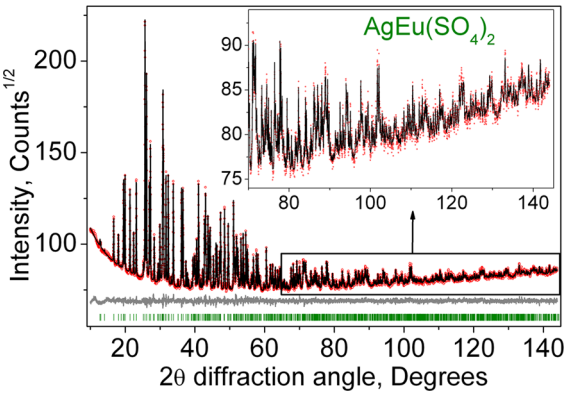

Figure 1. Measured (red), calculated (black), and differential (blue) diffraction patterns of $AgEu(SO_4)_2$.

indexed by primitive triclinic cell (a = 0.6321, b = 0.6899, c = 0.7048 nm, α = 98.96, β = 84.56, γ = 88.82°, V = 0.30203 nm^3, GoF = 44.1). Only two space groups can be suggested: $P\bar{1}$ or $P1$. First, the $P\bar{1}$ group was chosen as a model. The crystal structure was solved using a simulated annealing procedure applied to randomized coordinates of one Ag^+, one Eu^{3+} ion, and

DOI: 10.1021/acs.inorgchem.8b01837
Inorg. Chem. 2018, 57, 13279−13288

randomized coordinates with orientation angles of two SO_4^{2-} tetrahedra.[57] To merge the ions falling in special positions, the dynamical occupancy correction of the atoms was used.[57,58] The Monte Carlo algorithm quickly found the global minimum of *R*-factors and stopped at $R \approx 4\%$. The analysis of crystal structure revealed one Ag^+, one Eu^{3+}, and two independent SO_4 tetrahedra all in general positions (2i) (Figure 2). To reduce

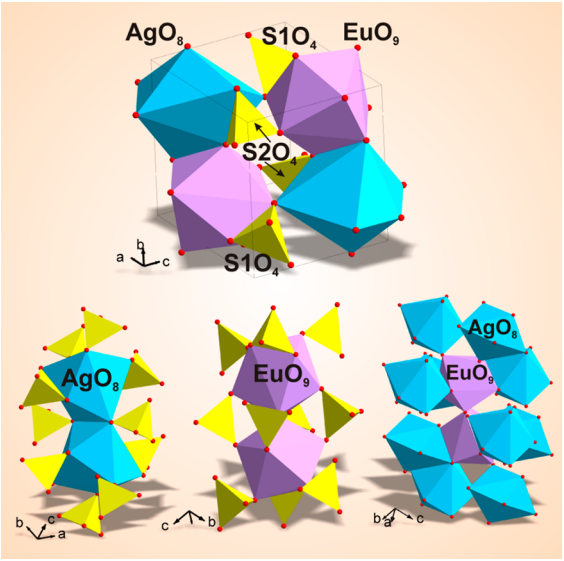

Figure 2. Crystal structure of $AgEu(SO_4)_2$.

number of refined parameters, it was suggested to refine only one thermal parameter for all O^{2-} ions and one thermal parameter for two S^{6+} ions. The refinement in the framework of this model was stable and gave low *R*-factors (Table 1, Figure 1).

Table 1. Main Parameters of Processing and Refinement of the Sample $AgEu(SO_4)_2$

compound	$AgEu(SO_4)_2$
space group	$P\bar{1}$
a, nm	0.632929(4)
b, nm	0.690705(4)
c, nm	0.705467(4)
α, °	98.9614(4)
β, °	84.5501(4)
γ, °	88.8201(4)
V, nm^3	0.303069(3)
Z	2
2θ interval, °	10–144
No. of reflections	1199
No. of refined parameters	83
R_{wp}, %	1.73
R_p, %	1.34
R_{exp}, %	1.18
χ^2	1.47
R_B, %	0.85

The coordinates of atoms and main bond lengths are listed in Tables 2 and 3, respectively. Checking of the $AgEu(SO_4)_2$ crystal structure with the program PLATON[59] did not reveal any problem, and this verifies the correct selection of space group $P\bar{1}$.

Further details of the crystal structure may be obtained from Fachinformationszentrum Karlsruhe, on quoting the deposition numbers: CSD-434695.

Table 2. Fractional Atomic Coordinates and Isotropic Displacement Parameters (nm^2)

atom	*x*	*y*	*z*	B_{iso}
Ag	0.9575(2)	0.6858(2)	0.2935(2)	0.0170(8)
Eu	0.3593(2)	0.8029(2)	0.7981(2)	0.0050(8)
S1	0.1270(8)	0.1792(7)	0.2056(7)	0.0100(8)
S2	0.4573(7)	0.7115(6)	0.2836(7)	0.0100(8)
O1	0.976(1)	0.026(1)	0.264(1)	0.010(1)
O2	0.264(1)	0.288(1)	0.354(1)	0.010(1)
O3	0.005(1)	0.323(1)	0.133(1)	0.010(1)
O4	0.324(1)	0.093(1)	0.060(1)	0.010(1)
O5	0.311(2)	0.698(1)	0.451(1)	0.010(1)
O6	0.568(1)	0.909(1)	0.326(1)	0.010(1)
O7	0.322(1)	0.694(1)	0.121(2)	0.010(1)
O8	0.621(1)	0.544(1)	0.264(1)	0.010(1)

Table 3. Main Bond Lengths (nm)[a]

Ag–O1^{i}	0.2402(8)	Eu–O5	0.249(1)
Ag–O2^{ii}	0.272(1)	Eu–O6^{vii}	0.2329(8)
Ag–O3^{iii}	0.2584(8)	Eu–O7^{viii}	0.250(1)
Ag–O3^{iv}	0.2988(9)	Eu–O8^{ii}	0.2365(8)
Ag–O5^{iii}	0.259(1)	S1–O1	0.148(1)
Ag–O6	0.2854(9)	S1–O2	0.154(1)
Ag–O7^{iii}	0.251(1)	S1–O3	0.143(1)
Ag–O8	0.2374(9)	S1–O4	0.158(1)
Eu–O1^{v}	0.257(1)	S2–O5	0.145(1)
Eu–O2^{ii}	0.254(1)	S2–O6	0.1549(9)
Eu–O3^{v}	0.251(1)	S2–O7	0.149(1)
Eu–O4^{vi}	0.2495(8)	S2–O8	0.1521(9)
Eu–O4^{ii}	0.240(1)		

[a]Symmetry codes for: (i) *x*, *y* + 1, *z*; (ii) −*x* + 1, −*y* + 1, −*z* + 1; (iii) *x* + 1, *y*, *z*; (iv) −*x* + 1, −*y* + 1, −*z*; (v) −*x*, −*y* + 1, −*z* + 1; (vi) *x*, *y* + 1, *z* + 1; (vii) −*x* + 1, −*y* + 2, −*z* + 1; (viii) *x*, *y*, *z* + 1.

The bond valence sum calculated for Eu^{3+} using values r_0 = 0.2076 nm, b_0 = 0.37,[60] and nine bond lengths *d*(Eu–O) in the range of (0.2329(8)– 0.257(1) nm) gave the value $BVS(Eu^{3+})$ = 3.20(9) that is close to 3+ formal valence state of Eu ion. Taking into account all these nine coordinations to O ions, one can build EuO_9 three-capped trigonal prism. The similar bond valence sum calculations made for all S^{6+} ions using r_0 = 0.1624 nm, b_0 = 0.37[60] gave BVS(S1) = 5.6(2) and BVS(S2) = 5.6(2), which are in good agreement (within 3σ of esd's interval) with 6+ valence state of S ions. The bond valence calculations performed for the Ag^+ ion using parameters r_0 = 0.1804 nm, b_0 = 0.37[60] and 8 bond lengths in the range of (0.2374(9)–0.2988(9) nm) gave $BVS(Ag^+)$ = 0.99(2) which is close to 1+ formal valence state of Ag^+ ion. The charge of all cations in the unit cell is 15.4(4), which deviates from the formal 16 expected but within 2σ interval. As far as estimated standard deviation of bond valence sum can be calculated using approximate formula $\sigma(BVS) \approx BVS\sigma(d)/b_0$, where BVS is bond valence sum, b_0 = 0.37, and $\sigma(d)$ is average estimated standard deviation of measured bond lengths, one can see linear relationship between σ(BVS) and $\sigma(d)$ of bond lengths. In our case, Rietveld refinement did not give very precise coordinates of light ions like O^{2-}, and bond lengths have relatively big $\sigma(d)$, which lead to relatively big σ(BVS). The AgO_8 polyhedron can be classified as bicapped trigonal prism. It is coordinated by two chelate bonded SO_4 tetrahedra, four monodentate bonded SO_4 tetrahedra, and another AgO_8 bonded by edge (Figure 2). The EuO_9 polyhedron is coordinated by two chelate bonded SO_4 tetrahedra

DOI: 10.1021/acs.inorgchem.8b01837
Inorg. Chem. 2018, 57, 13279–13288

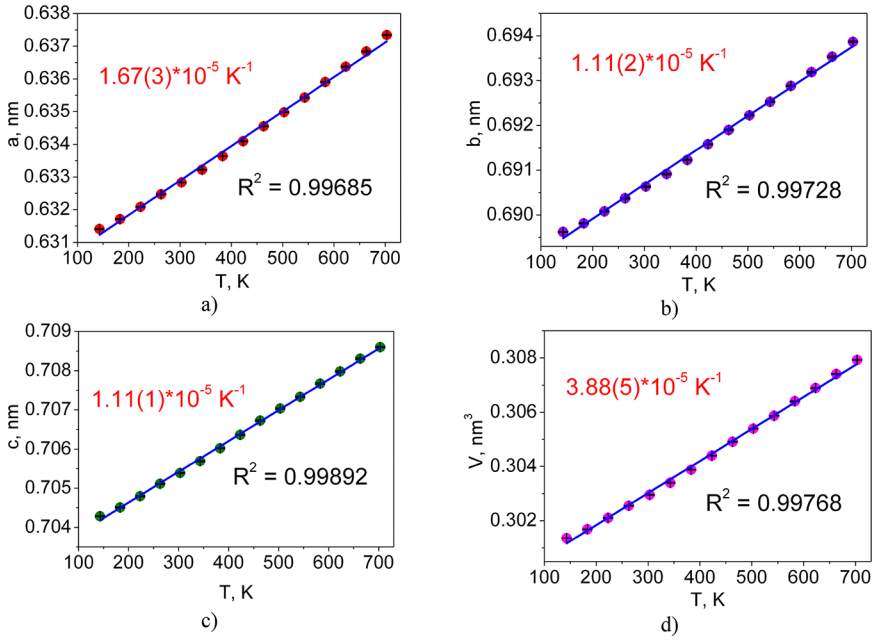

Figure 3. Cell parameters as a function of temperature T: (a) a(T); (b) b(T); (c) c(T); (d) V(T).

and five monodentate bonded SO_4 tetrahedra. The EuO_9 groups are joined with each other by edges forming a cluster, and each EuO_9 is coordinated by two chelate bonded AgO_8 polyhedra and three monodentate bonded AgO_8 polyhedra (Figure 2). In total, the EuO_9 polyhedron is double-edge connected. Therefore, all structural elements form a 3D net. The topological analysis of the net in ToposPro program,[61] using the simplification that the EuO_9, AgO_8, $S1O_4$, and $S2O_4$ groups are nodes, revealed that this is a 4-nodal (6-c)(7-c)(12-c)(13-c) net with point symbol $(3^{16}.4^{31}.5^{17}.6^2)(3^{17}.4^{34}.5^{23}.6^4)(3^6.4^9)(3^9.4^{12})$, which is new.

It is interesting to compare the structure of $AgEu(SO_4)_2$ with those of other triclinic sulfates listed in Table S1. The comparison of structures $NaLa(SO_4)_2$, $NaNd(SO_4)_2$, $AgPr(SO_4)_2$, $KPr(SO_4)_2$, $KNd(SO_4)_2$, and $AgEu(SO_4)_2$ provides the attribution of all the compounds to the $KPr(SO_4)_2$-type family. The situation with triclinic $AgEr(SO_4)_2$ is less clear because the available cell parameters are drastically different from these of $KPr(SO_4)_2$, and the structure of $AgEr(SO_4)_2$ was not reported on in the literature. Thus, the classification of the $AgEr(SO_4)_2$ structure is conjectural. The wide variation of the unit cell parameters should be mentioned in the $KPr(SO_4)_2$-type compounds, and this seems to be a specific feature of this structural family. Besides, on the basis of effective ion radii relation, the existence of triclinic $Tl^{I}Ln(SO_4)_2$ can be predicted.

The thermophysical properties of $AgEu(SO_4)_2$ were evaluated over the temperature range of 143−703 K, and the dependencies of unit cell parameters on temperature are shown in Figure 3. As seen, heating of the sample from 143 to 703 K leads to a continuous increase of all cell parameters (Table S2). The average linear thermal expansion coefficients of cell parameters a, b, and c are very similar (Figure 3) and, therefore, the compound expands almost isotropically. Above this, there is no prerequisite for a phase transition on the temperature decrease in triclinic $AgEu(SO_4)_2$ because disordered groups are absent in the structure. The representative SEM pattern recorded for the $AgEu(SO_4)_2$ sample is shown in Figure 4. According to the SEM observation, the product obtained as a result of solid state

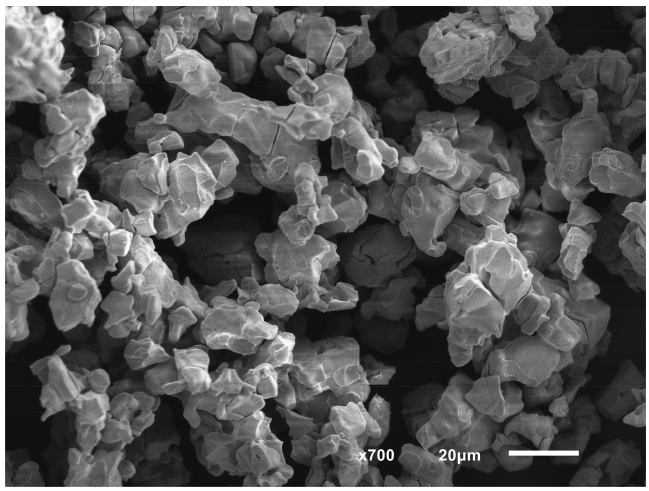

Figure 4. SEM pattern of $AgEu(SO_4)_2$.

reaction contains irregular particles 10−30 μm in diameter. The clear faceting was not detected for the particles.

To evaluate the solid-phase interaction between Ag_2SO_4 and $Eu_2(SO_4)_3$ used as starting materials as well as to see the stability of the formed double sulfate $AgEu(SO_4)_2$, the behavior of an equimolar mixture of Ag_2SO_4 and $Eu_2(SO_4)_3$ (Figure 5a) and stoichiometric $AgEu(SO_4)_2$ (Figure 5b) on heating in the air was studied by differential scanning calorimetry (DSC). The thermograms contains a large number of thermal effects, among them, several effects are known (A, D, E, and F).[62−67] The effects B and C are observed for the first time in the present study. The interpretation of thermal effects and corresponding reactions are given in Table 4. According to the thermogram shown in Figure 5a, no changes appeared in the starting sulfate mixture up to 697 K. At 697.5 K, an endothermic peak (A) was detected. However, the sample mass does not change. According to the literature, this transformation corresponds to a polymorphous transition of the rhombic modification of silver sulfate to hexagonal form.[62−65] The exothermic peak (B) originating at 874.5 K is not accompanied by a change in the sample mass.

DOI: 10.1021/acs.inorgchem.8b01837
Inorg. Chem. 2018, 57, 13279−13288

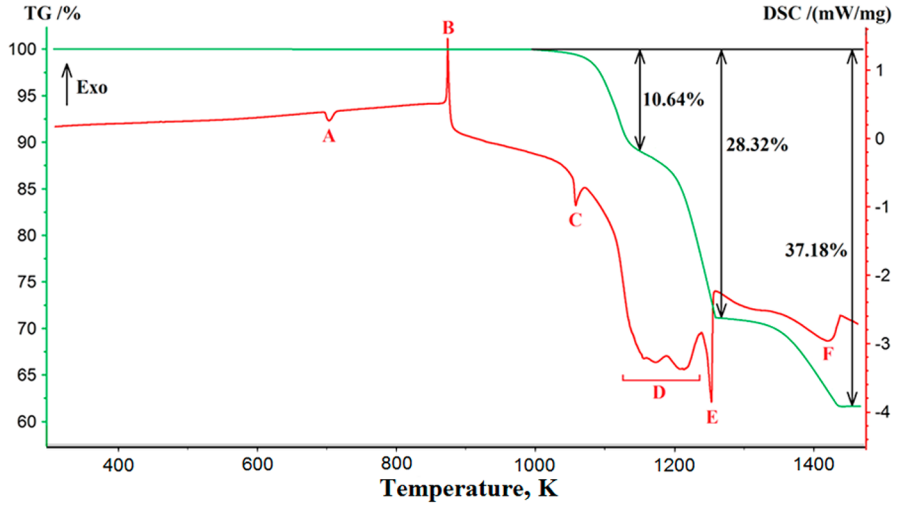

a

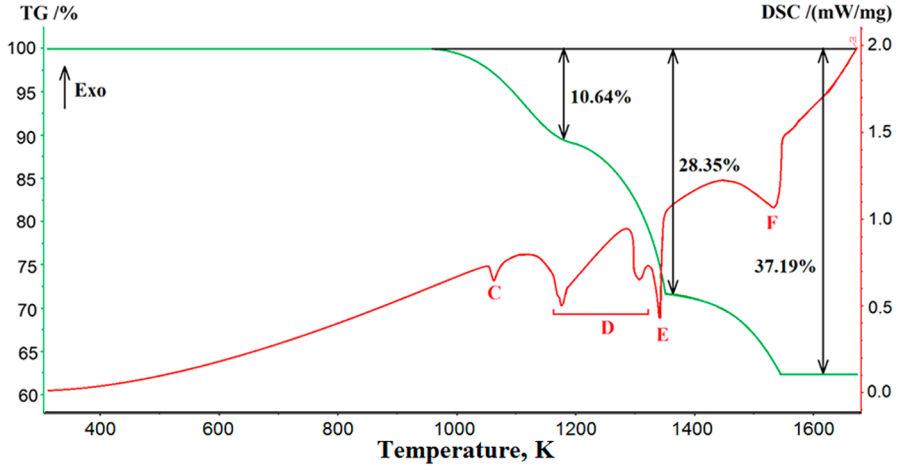

b

Figure 5. TG/DSC curves recorded for the (a) sulfate mixture (Ag_2SO_4 + $Eu_2(SO_4)_3$) and (b) stoichiometric $AgEu(SO_4)_2$.

Table 4. Thermal Effects in the Sulfate Mixture (Ag_2SO_4 + $Eu_2(SO_4)_3$) and Stoichiometric $AgEu(SO_4)_2$

thermal effect	reaction	ref
A	β-$Ag_2SO_{4(rhomb)} \rightarrow \alpha$-$Ag_2SO_{4(hexagon)}$	62−65
B	$Ag_2SO_4 + Eu_2(SO_4)_3 \rightarrow 2AgEu(SO_4)_2$	this work
C	$2AgEu(SO_4)_2 \rightarrow 2Ag + Eu_2(SO_4)_3 + SO_2 + O_2$	this work
D	$Eu_2(SO_4)_3 \rightarrow Eu_2O_2SO_4 + 2SO_2 + O_2$	15
E	$Ag_{(sol)} \rightarrow Ag_{(liq)}$	66, 67
F	$Eu_2O_2SO_4 \rightarrow Eu_2O_3 + SO_2 + {}^{1/2}O_2$	15

Earlier, when Ag_2SO_4 and $Eu_2(SO_4)_3$ were studied individually, no similar effect was observed.[15,64] Accounting for this, the effect (B) is interpreted as a chemical interaction of the Ag_2SO_4 and $Eu_2(SO_4)_3$ components, leading to the formation of a new complex sulfate $AgEu(SO_4)_2$.

The group of peaks (C−F) describing the process of complete decomposition of the compound $AgEu(SO_4)_2$ is found in the temperature range of 1053−1473 K. At 1058.2 K, an endothermic peak (C) is recorded, which obviously corresponds to the decay of the compound $AgEu(SO_4)_2$ into the original components. The silver sulfate released under this temperature is unstable and decomposes with the formation of metallic silver. This decomposition character is fully confirmed by the mass loss data. The further course of the decomposition process (D) is associated with the destruction of $Eu_2(SO_4)_3$ resulting in the formation of europium oxysulfate $Eu_2O_2SO_4$. The exothermic peak (E) is caused by the melting of metallic silver. The mass loss in the temperature range of 1273−1473 K (Figure 5a) and 1364−1557 K (Figure 5b) (peak F) is caused by decomposition of $Eu_2O_2SO_4$ to the oxide Eu_2O_3.

In both measured cases, $AgEu(SO_4)_2$ demonstrates practically the same thermal stability. However, after initiation of the thermal destruction, the process proceeds in different ways. The stoichiometric sample was subjected to a long annealing, resulting in their increased crystallinity. The process of stoichiometric sample decomposition is strongly kinetically hindered, and its complete destruction process is longer. Obviously, the thermal stability of the compound is determined by the deformation factors of the crystal structure. However, different kinetic parameters of the $AgEu(SO_4)_2$ decomposition indicate a significant role of size effects in this case.

The Raman and infrared spectra from $AgEu(SO_4)_2$ are shown in Figure 6. The vibrational representation for the triclinic phase at the Brillouin zone center is $\Gamma_{vibr} = 36A_g + 36A_u$ where acoustic modes are $\Gamma_{acoustic} = 3A_u$ and the remaining modes are optical.

DOI: 10.1021/acs.inorgchem.8b01837
Inorg. Chem. 2018, 57, 13279−13288

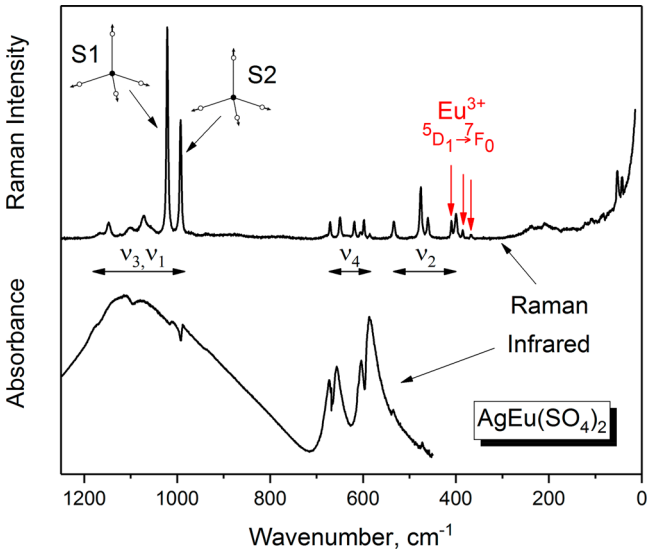

Figure 6. Raman and infrared spectra of $AgEu(SO_4)_2$.

Raman active modes are labeled g modes; infrared active modes are labeled u modes. Table 5 shows the correlation between the

Table 5. Correlation Diagram between T_d Point Symmetry, C_1 Sites Symmetry, and C_i Factor Group Symmetry for SO_4 Tetrahedra

wavenumber, cm^{-1}[70]	T_d point group	C_1 site symmetry	C_i factor group symmetry
983	A_1 (ν_1)	A	$A_g + A_u$
450	$E(\nu_2)$	$2A$	$2A_g + 2A_u$
1105	$F_2(\nu_3)$	$3A$	$3A_g + 3A_u$
611	$F_2(\nu_4)$	$3A$	$3A_g + 3A_u$

free SO_4 group with T_d symmetry, sites symmetry, and factor group symmetry of unit cell.[68] Taking into account that $AgEu(SO_4)_2$ has two crystallographically independent SO_4 tetrahedra, we can conclude that eight vibrational modes can appear in the range of stretching vibrations: two of them are symmetric stretching, and six ones antisymmetric stretching modes. The bending modes consist of six antisymmetric and four symmetric bending modes.

The calculation of $AgEu(SO_4)_2$ lattice dynamics using the program package LADY[69] was done to perform the interpretation of vibrational spectra. The atomic vibration values were obtained using the simplified version of the Born−Karman model.[70] Within this model, only the pairwise interactions and bond-stretching force constants F are considered, and the model implies that F depends on r_{ij} (interatomic distance). The dependencies $F(r_{ij})$ are the same for all atom pairs: $F(r_{ij}) = \lambda\exp(-r_{ij}/\rho)$, where λ and ρ are the parameters characterizing selected pair interaction. To find the parameters of the model, the special optimization program was written and tested for several representative compounds.[23,25,50,71−80] The crystal lattice stability conditions were taken into account. The parameters obtained for $AgEu(SO_4)_2$ are shown in Table S3.

The calculations show that 8 A_g and 8 A_u vibrational modes are in the region of SO_4 stretching, and 10 A_g and 10 A_u vibrational modes are in the region of SO_4 bending that is in agreement with the group-theoretical analysis. The complete set of calculated wavenumbers in comparison with experimental data is summarized in Table 6. Two high-wavenumber bands at

Table 6. Calculated Wavenumbers versus Experimental Raman and Infrared Data

Raman		infrared		
exp., cm^{-1}	A_g (calcd), cm^{-1}	exp., cm^{-1}	A_u (calcd), cm^{-1}	assignment
1166.2(6)	1199	1181(3)	1198	ν_3 SO_4
1147.6(1)	1198		1175	
	1139	1123(4)	1138	
1101.1(3)	1107		1115	
1072.2(2)	1048	1073(3)	1073	
1055.9(5)	1028		1030	
1021.36(5)	1000	1011(2)	1006	ν_1 SO_4
992.70(1)	975	984(1)	958	
670.91(5)	686	676.7(5)	699	ν_4 SO_4
649.47(3)	677	654.6(5)	641	
618.82(4)	625	605.9(4)	600	
605.6(1)	587	581.0(2)	560	
598.15(3)	546		538	
585.5(2)	538		522	
533.62(3)	500	533.8(2)	448	ν_2 SO_4
475.85(1)	429	471.6(2)	436	
460.33(3)	421		390	
409.74(3)				lum. Eu^{3+}
400.00(2)	392		360	ν_2 SO_4
385.40(5)				lum. Eu^{3+}
367.3(1)				
239.2(5)	293		311	rot. SO_4
	281		290	
	248		263	
	233		256	
222.8(6)	222		216	rot.+ transl. SO_4
209.1(9)	215		190	
197(2)	200		174	
184.3(9)	183		166	
164.1(9)	152		127	
148.2(9)	133		118	
121.5(3)	112		83	
108.3(3)	101			
	78			mixed vibr. transl. Ag, Eu
85.5(3)	57		78	
69.4(5)	51		61	
52.69(3)	48		52	
42.68(4)	42		51	
	39			

922 and 1024 cm^{-1} in Raman spectra are assigned to symmetric stretching of $S(2)O_4$ and $S(1)O_4$ tetrahedra, respectively. The other lines in the high-wavenumber region are antisymmetric stretching vibrations of SO_4. The shortest S(1)−O3 bond gives the highest wavenumber of antisymmetric vibrations. The symmetric and antisymmetric stretching vibrations in the infrared spectra are observed in the range of 975−1185 cm^{-1}.

In the Raman spectrum, 6 lines in the range of 585−670 cm^{-1} are ν_4 bending vibrations of SO_4 groups. The region of Raman spectrum between 360 and 560 cm^{-1} consists of 7 lines; according to lattice dynamics simulation, the lines at 533, 475, 460, and 400 cm^{-1} are ν_2 bending vibrations of SO_4, and the remaining lines at 367, 385, and 409 cm^{-1} are a triplet of luminescent lines $^5D_1$−$^7F_0$ of Eu^{3+} ion. The ν_2 and ν_4 bending vibrations of SO_4 were observed in the experimental infrared spectra below 700 cm^{-1}. A set of 18 A_g modes can be expected in the Raman low-frequency range. The vibrational modes of SO_4

DOI: 10.1021/acs.inorgchem.8b01837
Inorg. Chem. 2018, 57, 13279−13288

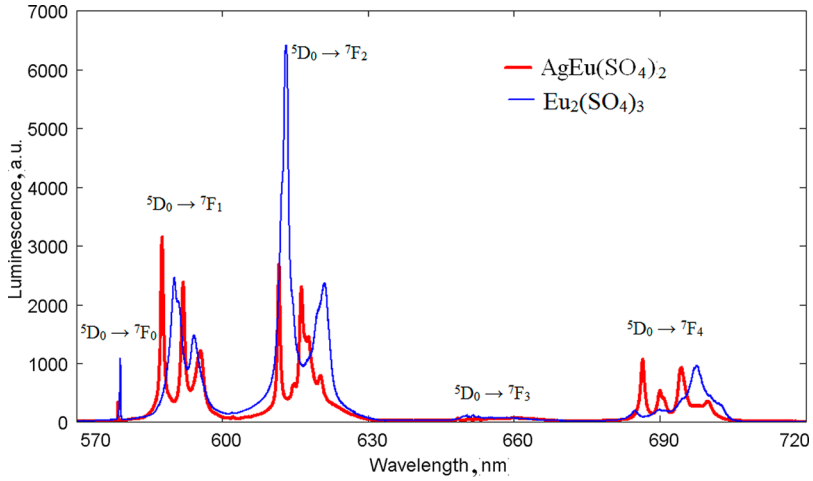

Figure 7. High resolution luminescence spectra of $AgEu(SO_4)_2$ (red) and of the reference crystal ($Eu_2(SO_4)_3$) (blue) excited at 514.5 nm.

tetrahedra in the 230−295 cm^{-1} range are assigned to rotational modes. The 100−230 cm^{-1} range of vibrational spectrum can be described as a combination of translation and vibrational modes of SO_4 tetrahedra. The translations of Ag, Eu, and mixed vibrations are below 100 cm^{-1}.

The overall high-resolution luminescence spectrum of $AgEu(SO_4)_2$ excited at 514.5 nm is plotted in Figure 7 in comparison with that from a reference crystal (anhydrous europium sulfate $Eu_2(SO_4)_3$).[81] Both spectra contain typical emission bands from $^5D_0$ state to spin−orbit components of ^7F multiplet. The luminescence intensity distribution between the bands both in $AgEu(SO_4)_2$ and in the reference crystal are in close similarity; however, certain differences can be detected. While in the reference crystal the hypersensitive transition $^5D_0 \rightarrow {}^7F_2$ dominates, in $AgEu(SO_4)_2$ the $^5D_0 \rightarrow {}^7F_1$ transition exhibits noticeably higher peak intensity with integral intensities of these two transitions in $AgEu(SO_4)_2$ being approximately the same. Therefore, parity breaking effect of the local environment onto the Eu ion in $AgEu(SO_4)_2$ is still present but is weaker than that in $Eu_2(SO_4)_3$. Additionally, the crystal field splitting of all transitions in $AgEu(SO_4)_2$ (naturally, except for the ultranarrow one) is larger than that in the reference crystal. The ultranarrow transition $^5D_0 \rightarrow {}^7F_0$ is clearly seen (Figure S2) in $AgEu(SO_4)_2$, which is consistent with the local symmetry of Eu^{3+} ion within this new triclinic structure, being as low as C_1. However, the amplitude of the ultranarrow peak in $AgEu(SO_4)_2$ is three times smaller than that in $Eu_2(SO_4)_3$. Therefore, the effect of the violation of the mirror symmetry at the europium site in $AgEu(SO_4)_2$ is weaker than that in $Eu_2(SO_4)_3$. At the same time, the shape of the ultranarrow line in $AgEu(SO_4)_2$ is almost perfectly symmetric, in contrast to clearly asymmetric line shape of this transition in $Eu_2(SO_4)_3$. As a result, the line width at $^5D_0 \rightarrow {}^7F_0$ transition is smaller in $AgEu(SO_4)_2$. These observations can be treated as evidence for the good crystalline quality of $AgEu(SO_4)_2$ and the homogeneity of Eu^{3+} ion environment. At the same time, the influence of Ag^+ ions on the electron density distribution at Eu^{3+} ion sites can be evidenced by the blue shift of ultranarrow line position to 578.5 nm in $AgEu(SO_4)_2$.

CONCLUSIONS

In the presented study, the structural, spectroscopic, and thermal properties of the new silver−europium double sulfate $AgEu(SO_4)_2$ were studied for the first time. To obtain a pure sample, a solid-phase reaction was used between simple sulfates. To date, it is important to develop a technique of production based on the methods of "soft chemistry". It is established that the compound crystallizes in space group $P\bar{1}$. Several compounds with similar structure have been earlier found and, therefore, the $AgEu(SO_4)_2$ is classified as a member of $KPr(SO_4)_2$-type family. The topological analysis of this class of compounds was performed for the first time, and it revealed that the simplified 3D net is new. When switching to compounds of heavy rare-earth elements, a change of structural type should be expected. Heating of the sample did not lead to any phase transition; the cell parameters *a*, *b*, and *c* increase with temperature increase, and the dependences can be approximated by linear functions. The corresponding average linear thermal expansion coefficients are very similar; therefore, the compound expands almost isotropically. The distribution of the luminescence intensity between the bands in $AgEu(SO_4)_2$ is in close similarity to that in previously studied $Eu_2(SO_4)_3$, but the parity violation effect of the local environment in $AgEu(SO_4)_2$ is less pronounced than that in $Eu_2(SO_4)_3$.

ASSOCIATED CONTENT

Supporting Information

The Supporting Information is available free of charge on the ACS Publications website at DOI: 10.1021/acs.inorgchem.8b01837.

Sample photo image, luminescence spectra, structural information, and parameters of the interatomic interaction potential (PDF)

Accession Codes

CCDC 1855256 contains the supplementary crystallographic data for this paper. These data can be obtained free of charge via www.ccdc.cam.ac.uk/data_request/cif, by emailing data_request@ccdc.cam.ac.uk, or by contacting The Cambridge Crystallographic Data Centre, 12 Union Road, Cambridge CB2 1EZ, UK; fax: +44 1223 336033.

AUTHOR INFORMATION

Corresponding Author

*Phone: +7 (383) 3308889; E-mail: atuchin@isp.nsc.ru.

ORCID

Victor V. Atuchin: 0000-0002-7424-5604

Aleksandr S. Aleksandrovsky: 0000-0003-1821-6718

Notes

The authors declare no competing financial interest.

DOI: 10.1021/acs.inorgchem.8b01837
Inorg. Chem. 2018, 57, 13279−13288

■ ACKNOWLEDGMENTS

This work was supported by the Russian Foundation for Basic Research (Grants 16-52-48010 and 17-52-53031). The equipment of the Collective Use Center, Kirensky Institute of Physics, Federal Research Center KSC Siberian Branch Russian Academy of Sciences (http://ccu.kirensky.ru/) were used.

■ REFERENCES

(1) Sun, L.-D.; Wang, Y.-F.; Yan, C.-H. Paradigms and Challenges for Bioapplication of Rare Earth Upconversion Luminescent Nanoparticles: Small Size and Tunable Emission/Excitation Spectra. *Acc. Chem. Res.* **2014**, *47*, 1001−1009.

(2) Li, G.; Tian, Y.; Zhao, Y.; Lin, J. Recent Progress in Luminescence Tuning of Ce^{3+} and Eu^{2+}-activated Phosphors for pc-WLEDs. *Chem. Soc. Rev.* **2015**, *44*, 8688−8713.

(3) Kaczmarek, A. M.; Van Hecke, K.; Van Deun, R. Nano-and Microsized Rare-earth Carbonates and their Use as Precursors and Sacrificial Templates for the Synthesis of New Innovative Materials. *Chem. Soc. Rev.* **2015**, *44*, 2032−2059.

(4) Atuchin, V. V.; Beisel, N. F.; Galashov, E. N.; Mandrik, E. M.; Molokeev, M. S.; Yelisseyev, A. P.; Yusuf, A. A.; Xia, Z. Pressure-stimulated Synthesis and Luminescence Properties of Microcrystalline $(Lu,Y)_3Al_5O_{12}:Ce^{3+}$ Garnet Phosphors. *ACS Appl. Mater. Interfaces* **2015**, *7*, 26235−26243.

(5) Xia, Z.; Liu, Q. Progress in Discovery and Structural Design of Color Conversion Phosphors for LEDs. *Prog. Mater. Sci.* **2016**, *84*, 59−117.

(6) Karthik, R.; Kumar, J. V.; Chen, S.-M.; Kokulnathan, T.; Yang, H.-Y.; Muthuraj, V. Design of Novel Ytterbium Molybdate Nano-flakes Anchored Carbon Nanofibers: A Challenging Sustainable Catalyst for the Detection and Degradation of Assassination Weapon (Paraoxon-ethyl). *ACS Sustainable Chem. Eng.* **2018**, *6*, 8615−8630.

(7) Ponomarev, B. K. Magneto-electrical Properties of Rare Earth Molybdates. *Ferroelectrics* **2002**, *280*, 95−117.

(8) Wickleder, M. S. Inorganic Lanthanide Compounds with Complex Anions. *Chem. Rev.* **2002**, *102*, 2011−2087.

(9) Shi, P.; Xia, Z.; Molokeev, M. S.; Atuchin, V. V. Crystal Chemistry and Luminescence Properties of Red-emitting $CsGd_{1-x}Eu_x(MoO_4)_2$ Solid Solution Phosphors. *Dalton Trans.* **2014**, *43*, 9669−9676.

(10) Golovnev, N. N.; Molokeev, M. S.; Vereshchagin, S. N.; Atuchin, V. V. Synthesis and Thermal Transformation of a Neodymium (III) Complex $[Nd(HTBA)_2(C_2H_3O_2)(H_2O)_2]\cdot 2H_2O$ to Non-centrosymmetricoxosulfate $Nd_2O_2SO_4$. *J. Coord. Chem.* **2015**, *68*, 1865−1877.

(11) Atuchin, V. V.; Aleksandrovsky, A. S.; Chimitova, O. D.; Diao, C.-P.; Gavrilova, T. A.; Kesler, V. G.; Molokeev, M. S.; Krylov, A. S.; Bazarov, B. G.; Bazarova, J. G.; Lin, Z. Electronic Structure of β-$RbSm(MoO_4)_2$ and Chemical Bonding in Molybdates. *Dalton Trans.* **2015**, *44*, 1805−1815.

(12) Reshak, A. H.; Alahmed, Z. A.; Bila, J.; Atuchin, V. V.; Bazarov, B. G.; Chimitova, O. D.; Molokeev, M. S.; Prosvirin, I. P.; Yelisseyev, A. P. Exploration of the Electronic Structure of Monoclinic α-$Eu_2(MoO_4)_3$: DFT-based Study and X-ray Photoelectron Spectroscopy. *J. Phys. Chem. C* **2016**, *120*, 10559−10568.

(13) Fulle, K.; Sanjeewa, L. D.; McMillen, C. D.; Kolis, J. W. Crystal Chemistry and the Role of Ionic Radius in Rare Earth Tetrasilicates: $Ba_2RE_2Si_4O_{12}F_2$ (RE= Er^{3+}−Lu^{3+}) and $Ba_2RE_2Si_4O_{13}$ (RE= La^{3+}−Ho^{3+}). *Acta Crystallogr., Sect. B: Struct. Sci., Cryst. Eng. Mater.* **2017**, *73*, 907−915.

(14) Chakhmouradian, A. R.; Cooper, M. A.; Reguir, E. P.; Moore, M. A. Carbocernaite from Bear Lodge, Wyoming: Crystal Chemistry, Paragenesis, and Rare-earth Fractionation on a Microscale. *Am. Mineral.* **2017**, *102*, 1340−1352.

(15) Denisenko, Yu. G.; Khritokhin, N. A.; Andreev, O. V.; Basova, S. A.; Sal'nikova, E. I.; Polkovnikov, A. A. Thermal Decomposition of Europium Sulfates $Eu_2(SO_4)_3\cdot 8H_2O$ and $EuSO_4$. *J. Solid State Chem.* **2017**, *255*, 219−224.

(16) Aughterson, R. D.; Lumpkin, G. R.; Smith, K. L.; Zhang, Z.; Sharma, N.; Cairney, J. M. The Crystal Structures and Corresponding Ion-irradiation Response for the $Tb_{(x)}Yb_{(2-x)}TiO_5$ Series. *Ceram. Int.* **2018**, *44*, 511−519.

(17) Kaminskii, A. A.; Gruber, J. B.; Bagaev, S. N.; Ueda, K.; Hömmerich, U.; Seo, J. T.; Temple, D.; Zandi, B.; Kornienko, A. A.; Dunina, E. B.; Pavlyuk, A. A.; Klevtsova, R. F.; Kuznetsov, F. A. Optical Spectroscopy and Visible Stimulated Emission of Dy^{3+} Ions in Monoclinic α-$KY(WO_4)_2$ and α-$KGd(WO_4)_2$ Crystals. *Phys. Rev. B: Condens. Matter Mater. Phys.* **2002**, *65*, 125108.

(18) Atuchin, V. V.; Pokrovsky, L. D.; Khyzhun, O. Y.; Sinelnichenko, A. K.; Ramana, C. V. Surface Crystallography and Electronic Structure of Potassium Yttrium Tungstate. *J. Appl. Phys.* **2008**, *104*, 033518.

(19) Mączka, M.; Hermanowicz, K.; Kępiński, L.; Hanuza, J.; Yordanova, A.; Koseva, L. Raman Spectroscopy and Optical Properties of Nanocrystalline $NaAl(WO_4)_2:Cr^{3+}$ Powder Prepared by Co-precipitation/Calcination Method. *Opt. Mater.* **2013**, *35*, 338−346.

(20) Atuchin, V. V.; Chimitova, O. D.; Adichtchev, S. V.; Bazarov, B. G.; Gavrilova, T. A.; Molokeev, M. S.; Surovtsev, N. V.; Bazarova, Zh. G. Synthesis, Structural and Vibrational Properties of Microcrystalline β-$RbSm(MoO_4)_2$. *Mater. Lett.* **2013**, *106*, 26−29.

(21) Lim, C. S.; Aleksandrovsky, A.; Molokeev, M.; Oreshonkov, A.; Atuchin, V. Microwave Sol-gel Synthesis and Upconversion Photoluminescence Properties of $CaGd_2(WO_4)_4:Er^{3+}/Yb^{3+}$ Phosphors with Incommensurately Modulated Structure. *J. Solid State Chem.* **2015**, *228*, 160−166.

(22) Lim, C. S. Highly Modilated Structure and Upconversion Photoluminescence Properties of $PbGd_2(MoO_4)_4:Er^{3+}/Yb^{3+}$ Phosphors. *Mater. Res. Bull.* **2016**, *75*, 211−216.

(23) Lim, C. S.; Aleksandrovsky, A. S.; Molokeev, M. S.; Oreshonkov, A. S.; Atuchin, V. V. Microwave Synthesis and Spectroscopic Properties of Ternary Scheelite-type Molybdate Phosphors $NaSrLa(MO_4)_3:Er^{3+}/Yb^{3+}$. *J. Alloys Compd.* **2017**, *713*, 156−163.

(24) Pietrelli, L.; Bellomo, B.; Fontana, D.; Montereali, M. R. Rare Earths Recovery from NiMH Spent Batteries. *Hydrometallurgy* **2002**, *66*, 135−139.

(25) Li, D.; Zuo, Y.; Meng, S. Separation of Thorium (IV) and Extracting Rare Earths from Sulfuric and Phosphoric Acid Solutions by Solvent Extraction Method. *J. Alloys Compd.* **2004**, *374*, 431−433.

(26) Kul, M.; Topkaya, Y.; Karakaya, I. Rare Earth Double Sulfates from Pre-concentrated Bastnasite. *Hydrometallurgy* **2008**, *93*, 129−135.

(27) Jun, T.; Jingqun, Y.; Ruan, C.; Guohua, R.; Mintao, J.; Kexian, O. Kinetics on Leaching Rare Earth from the Weathered Crust Elution-deposited Rare Earth Ores with Ammonium Sulfate Solution. *Hydrometallurgy* **2010**, *101*, 166−170.

(28) Beltrami, D.; Deblonde, G. J.-P.; Bélair, S.; Weigel, W. Recovery of Yttrium and Lanthanides from Sulfate Solutions with High Concentration of Iron and Low Rare Earth Content. *Hydrometallurgy* **2015**, *157*, 356−362.

(29) Zhu, Z.; Pranolo, Y.; Cheng, C. Y. Separation of Uranium and Thorium from Rare Earths for Rare Earth Production − A Review. *Miner. Eng.* **2015**, *77*, 185−196.

(30) Jha, M. K.; Kumari, A.; Panda, R.; Kumar, J. R.; Yoo, K.; Lee, J. Y. Review on Hydrometallurgical Recovery of Rare Earth Metals. *Hydrometallurgy* **2016**, *165*, 2−26.

(31) Diaz, L. A.; Lister, T. E.; Parkman, J. A.; Clark, G. G. Comprehensive Process for the Recovery of Value and Critical Materials from Electronic Waste. *J. Cleaner Prod.* **2016**, *125*, 236−244.

(32) Perles, J.; Fortes-Revilla, C.; Guttérrez-Puebla, E.; Iglesias, M.; Monge, M. A.; Ruiz-Valero, C.; Snejko, N. Synthesis, Structure, and Catalytic Properties of Rare-earth Ternary Sulfates. *Chem. Mater.* **2005**, *17*, 2701−2706.

(33) Deng, Z.; Bai, F.; Xing, Y.; Xing, N.; Xu, L. Reaction in situ Found in the Synthesis of a Series of Lanthanide Sulfate Complexes and Investigation on their Structure, Spectra and Catalytic Activity. *Open J. Inorg. Chem.* **2013**, *3*, 76−99.

(34) Sirotinkin, S. P.; Efremov, V. A.; Pokrovskii, A. N.; Kovba, L. M. Crystal Structure of Lithium Praseodymium Sulfate $LiPr(SO_4)_2$. *Kristallografiya* **1978**, *23*, 406−408.

DOI: 10.1021/acs.inorgchem.8b01837
Inorg. Chem. 2018, 57, 13279−13288

(35) Sirotinkin, S. P.; Efremov, V. A.; Kovba, L. M.; Pokrovskii, A. N. Crystal Structure of Lithium-europium Double Sulfate. *Kristallografiya* **1977**, *22*, 966−970.
(36) Sirotinkin, S. P.; Pokrovskii, A. N.; Kovba, L. M. Crystal Structures of Certain Double and Simple Rare Earth Sulfates. *Kristallografiya* **1981**, *26*, 385−389.
(37) Chizhov, S. M.; Pokrovskii, A. N.; Kovba, L. M. The Crystal Structure of $NaLa(SO_4)_2$. *Kristallografiya* **1981**, *26*, 834−836.
(38) Sirotinkine, S. P.; Tchijov, S. M.; Pokrovskii, A. N.; Kovba, L. M. Structure Cristalline de Sulfates Doubles de Sodium et de Terres Rares. *J. Less-Common Met.* **1978**, *58*, 101−105.
(39) Degtyarev, P. A.; Kovba, L. M.; Pokrovskii, A. N. Crystal Structure of the Anhydrous Double Sulfate $KPr(SO_4)_2$. *Kristallografiya* **1978**, *23*, 840−843.
(40) Degtyarev, P. A.; Korytnaya, F. M.; Kovba, L. M.; Pokrovskii, A. N. Crystal Structure of the Anhydrous Double Sulfate of Potassium and Neodymium $KNd(SO_4)_2$. *Vestnik Moskovskogo Universiteta − Khimiya* **1977**, *18*, 705−708.
(41) Iskhakova, L. D.; Gasanov, Y. M.; Trunov, V. K. Crystal Structure of the Monoclinic Modification of $KNd(SO_4)_2$. *J. Struct. Chem.* **1988**, *29*, 242−246.
(42) Bukovec, N.; Kaucic, V.; Golic, L. Cesium Lanthanum Bis(sulphate). *Acta Crystallogr., Sect. B: Struct. Crystallogr. Cryst. Chem.* **1980**, *36*, 129−130.
(43) Bukovec, N.; Golic, L.; Bukovec, P.; Siftar, J. Die Synthese und Kristallstruktur von Caesium-Praseodymsulfat. *Monatsh. Chem.* **1978**, *109*, 1305−1310.
(44) Ruiz-Valero, C.; Cascales, C.; Gómez-Lor, B.; Gutiérrez-Puebla, E.; Iglesias, M.; Monge, M. A.; Snejko, N. New Catalytically Active Neodymium Sulfate. *J. Mater. Chem.* **2002**, *12*, 3073−3077.
(45) Cheng, F.; Xia, Z.; Molokeev, M. S.; Jing, X. Effects of Composition Modulation on the Luminescence Properties of Eu^{3+} Doped $Li_{1-x}Ag_xLu(MoO_4)_2$ Solid Solution Phosphors. *Dalton Trans.* **2015**, *44*, 18078−18089.
(46) Wang, X.; Li, J.-G.; Molokeev, M. S.; Zhu, Q.; Li, X.; Sun, X. Layered Hydroxyl Sulfate: Controlled Crystallization, Structure Analysis, and Green Derivation of Multi-color Luminescent $(La,RE)_2O_2SO_4$ and $(La,RE)_2O_2S$ Phosphors (RE = Pr, Sm, Eu, Tb, and Dy). *Chem. Eng. J.* **2016**, *302*, 577−586.
(47) Loiko, P. A.; Vilejshikova, E. V.; Mateos, X.; Serres, J. M.; Dashkevich, V. I.; Orlovich, V. A.; Yasukevich, A. S.; Kuleshov, N. V.; Yumashev, K. V.; Grigoriev, S. V.; Vatnik, S. M.; Bagaev, S. N.; Pavlyuk, A. A. Spectroscopy of Tetragonal Eu:$NaGd(WO_4)_2$ Crystal. *Opt. Mater.* **2016**, *57*, 1−7.
(48) Wang, Y.; Wu, W.; Fu, X.; Liu, M.; Cao, J.; Shao, C.; Chen, S. Metastable Scheelite $CdWO_4$:Eu^{3+} Nanophosphors: Solvothermal Synthesis, Phase Transitions and their Polymorph-dependent Luminescence Properties. *Dyes Pigm.* **2017**, *147*, 283−290.
(49) Jaganathan, S. K.; Peter, A. J. Synthesis and Luminescence Properties of $CaGd_2(MoO_4)_4$:Ln^{3+} (Ln = Eu^{3+}, Tb^{3+}, Dy^{3+} and Sm^{3+}) Phosphors. *J. Lumin.* **2018**, *199*, 53−59.
(50) Atuchin, V. V.; Aleksandrovsky, A. S.; Chimitova, O. D.; Gavrilova, T. A.; Krylov, A. S.; Molokeev, M. S.; Oreshonkov, A. S.; Bazarov, B. G.; Bazarova, J. G. Synthesis and Spectroscopic Properties of Monoclinic α-$Eu_2(MoO_4)_3$. *J. Phys. Chem. C* **2014**, *118*, 15404−15411.
(51) Ji, H.; Huang, Z.; Xia, Z.; Molokeev, M. S.; Jiang, X.; Lin, Z.; Atuchin, V. V. Comparative Investigations of the Crystal Structure and Photoluminescence Property of Eulytite-type $Ba_3Eu(PO_4)_3$ and $Sr_3Eu(PO_4)_3$. *Dalton Trans.* **2015**, *44*, 7679−7686.
(52) Wang, X.; Molokeev, M. S.; Zhu, Q.; Li, J.-G. Controlled Hydrothermal Crystallization of Anhydrous $Ln_2(OH)_4SO_4$ (Ln = Eu-Lu, Y) as a New Family of Layered Rare Earth Hydrooxides. *Chem. - Eur. J.* **2017**, *23*, 16034−16043.
(53) Atuchin, V. V.; Subanakov, A. K.; Aleksandrovsky, A. S.; Bazarov, B. G.; Bazarova, J. G.; Gavrilova, T. A.; Krylov, A. S.; Molokeev, M. S.; Oreshonkov, A. S.; Stefanovich, S. Yu Structural and Spectroscopic Properties of Noncentrosymmetric Self-activated Borate $Rb_3EuB_6O_{12}$ with B_5O_{10} Units. *Mater. Des.* **2018**, *140*, 488−494.
(54) Tan, S.; Paglieri, S. N.; Li, D. Nano-scale Sulfur-tolerant Lanthanide Oxysulfide/Oxysulfate Catalysts for Water−gas-shift Reaction in a Novel Reactor Configuration. *Catal. Commun.* **2016**, *73*, 16−21.
(55) Krylov, A.; Vtyurin, A. N.; Petkov, P.; Senkovska, I.; Maliuta, M.; Bon, V.; Heine, T.; Kaskel, S.; Slyusareva, E. Raman Spectroscopy Studies of the Terahertz Vibrational Modes of a DUT-8 (Ni) Metal-organic Framework. *Phys. Chem. Chem. Phys.* **2017**, *19*, 32099−32104.
(56) Krylov, A.; Goryainov, S. V.; Vtyurin, A. N.; Krylova, S. N.; Sofronova, S. N.; Laptash, N. M.; Emelina, T. B.; Voronov, V. N.; Babushkin, S. V. Raman Scattering Study of Temperature and Hydrostatic Pressure Phase Transitions in Rb_2KTiOF_5 Crystal. *J. Raman Spectrosc.* **2012**, *43*, 577−582.
(57) Favre-Nicolin, V.; Cerny, R. FOX: Modular Approach to Crystal Structure Determination from Powder Diffraction. *Mater. Sci. Forum* **2004**, *443*, 35−38.
(58) Favre-Nicolin, V.; Cerny, R. FOX, Free Objects for Crystallography': a Modular Approach to ab initio Structure Determination from Powder Diffraction. *J. Appl. Crystallogr.* **2002**, *35*, 734−743.
(59) Spek, A. L. Single-crystal Structure Validation with the Program PLATON. *J. Appl. Crystallogr.* **2003**, *36*, 7−13.
(60) Brese, N. E.; O'Keeffe, M. Bond-valence Parameters for Solids. *Acta Crystallogr., Sect. B: Struct. Sci.* **1991**, *47*, 192−197.
(61) Blatov, V. A.; Shevchenko, A. P.; Proserpio, D. M. Applied Topological Analysis of Crystal Structures with the Program Package ToposPro. *Cryst. Growth Des.* **2014**, *14*, 3576−3586.
(62) Secco, R. A.; Secco, E. A. Structural and Nonstructural Factors in Fast Ion Conduction in Ag_2SO_4 at High Pressure. *Phys. Rev. B: Condens. Matter Mater. Phys.* **1997**, *56*, 3099−3104.
(63) Pistorius, C. W. F. T. Phase Diagrams of Silver Sulfate, Silver Selenate, and Silver Chromate to 40 kbar. *J. Chem. Phys.* **1967**, *46*, 2167−2171.
(64) Rao, S. R.; Lingam, C. B.; Rajesh, D.; Vijayalakshmil, R. P.; Sunandana, C. S. Thermal and Spectroscopy Studies of Ag_2SO_4 and $LiAgSO_4$. *IOSR J. Appl. Phys.* **2013**, *4*, 39−43.
(65) Larsen, H. B.; Thorkildsen, G.; Nicholson, D. G.; Pattison, P. Thermal Induced Structural Properties of Silver (I) Sulphate (Ag_2SO_4). *Cryst. Res. Technol.* **2016**, *51*, 730−737.
(66) Johnstone, J. K. Cryoscopic studies of the melting point of silver in high pressure oxygen. *J. Electrochem. Soc.* **1965**, *112*, 25C−27C.
(67) Speros, D. M.; Woodhouse, R. L. Realization of Quantitative Differential Thermal Analysis. I Heats and Rates of Solid-Liquid Transitions. *J. Phys. Chem.* **1963**, *67*, 2164−2168.
(68) Nakamoto, K. *Infrared and Raman Spectra of Inorganic and Coordination Compounds*, 6th ed.; Wiley: New York, 2009.
(69) Smirnov, M. B.; Kazimirov, V. Y. *LADY: Software for Lattice Dynamics Simulations*; JINR Communications, 2001.
(70) Smirnov, M.; Baddour-Hadjean, R. Li Intercalation in TiO_2 Anatase: Raman Spectroscopy and Lattice Dynamic Studies. *J. Chem. Phys.* **2004**, *121*, 2348−2355.
(71) Vtyurin, A. N.; Krylov, A. S.; Krylova, S. N.; Goryainov, S. V.; Voronov, V. N.; Oreshonkov, A. S. Hydrostatic Pressure-induced Phase Transitions in Rb_2KInF_6 and Rb_2KScF_6 Crystals: Raman Spectra and Lattice Dynamics Simulations. *Ferroelectrics* **2012**, *440*, 100−104.
(72) Krylov, A. S.; Vtyurin, A. N.; Oreshonkov, A. S.; Voronov, V. N.; Krylova, S. N. Structural Transformations in a Single-crystal Rb_2NaYF_6: Raman Scattering Study. *J. Raman Spectrosc.* **2013**, *44*, 763−769.
(73) Xia, Z.; Molokeev, M. S.; Oreshonkov, A. S.; Atuchin, V. V.; Liu, R.-S.; Dong, C. Crystal and Local Structure Refinement in $Ca_2Al_3O_6F$ Explored by X-ray Diffraction and Raman Spectroscopy. *Phys. Chem. Chem. Phys.* **2014**, *16*, 5952−5957.
(74) Lim, C. S.; Aleksandrovsky, A. S.; Molokeev, M. S.; Oreshonkov, A. S.; Atuchin, V. V. The Modulated Structure and Frequency Upconversion Properties of $CaLa_2(MoO_4)_4$:Ho^{3+}/Yb^{3+} Phosphors Prepared by Microwave Synthesis. *Phys. Chem. Chem. Phys.* **2015**, *17*, 19278−19287.
(75) Oreshonkov, A. S.; Gerasimova, J. V.; Ershov, A. A.; Krylov, A. S.; Shaykhutdinov, K. A.; Vtyurin, A. N.; Molokeev, M. S.; Terent'ev, K. Y.;

DOI: 10.1021/acs.inorgchem.8b01837
Inorg. Chem. 2018, 57, 13279−13288

Mihashenok, N. V. Raman Spectra and Phase Composition of $MnGeO_3$ Crystals. *J. Raman Spectrosc.* **2016**, *47*, 531−536.
(76) Lim, C. S.; Aleksandrovsky, A. S.; Molokeev, M. S.; Oreshonkov, A. S.; Ikonnikov, D. A.; Atuchin, V. V. Triple Molybdate Scheelite-type Upconversion Phosphor $NaCaLa(MoO_4)_3:Er^{3+}/Yb^{3+}$: Structural and Spectroscopic Properties. *Dalton Trans.* **2016**, *45*, 15541−15551.
(77) Oreshonkov, A. S.; Krylov, A. S.; Shestakov, N. P.; Voronov, V. N.; Ershov, A. A.; Strikina, E. A.; Vtyurin, A. N. Vibrational Spectra of NdF_3 Crystal. *Ferroelectrics* **2016**, *501*, 15−19.
(78) Strikina, E. A.; Krylov, A. S.; Oreshonkov, A. S.; Vtyurin, A. N. Raman Scattering Study of δ-BiB_3O_6 Crystal. *Ferroelectrics* **2016**, *501*, 26−31.
(79) Krylov, A. S.; Molokeev, M. S.; Misyul, S. V.; Krylova, S. N.; Oreshonkov, A. S.; Ivanenko, A. A.; Zykova, V. A.; Ivanov, Y. N.; Sukhovsky, A. A.; Voronov, V. N.; Safonov, I. N.; Vtyurin, A. N. Crystal Structure and Phase Transitions of a Layered Perovskite-like $CsScF_4$ Crystal. *CrystEngComm* **2016**, *18*, 8472−8486.
(80) Atuchin, V. V.; Aleksandrovsky, A. S.; Molokeev, M. S.; Krylov, A. S.; Oreshonkov, A. S.; Zhou, D. Structural and Spectroscopic Pproperties of Self-activated Monoclinic Molybdate $BaSm_2(MoO_4)_4$. *J. Alloys Compd.* **2017**, *729*, 843−849.
(81) Denisenko, Yu. G.; Aleksandrovsky, A. S.; Atuchin, V. V.; Krylov, A. S.; Molokeev, M. S.; Oreshonkov, A. S.; Shestakov, N. P.; Andreev, O. V. Exploration of Structural, Thermal and Spectroscopic Properties of Self-activated Sulfate $Eu_2(SO_4)_3$ with Isolated SO_4 Groups. *J. Ind. Eng. Chem.* **2018**, 1 DOI: 10.1016/j.jiec.2018.07.034.

DOI: 10.1021/acs.inorgchem.8b01837
Inorg. Chem. 2018, 57, 13279−13288